Proposed Method for Reconstructing Velocity Profiles Using a Multi-Electrode Electromagnetic Flow Meter

László E. Kollár*, Gary P. Lucas, Zhichao Zhang

School of Computing and Engineering, University of Huddersfield, UK

*Corresponding author: l.kollar@hud.ac.uk

Abstract

An analytical method is developed for the reconstruction of velocity profiles using measured potential distributions obtained around the boundary of a multi-electrode electromagnetic flow meter (EMFM). The method is based on the Discrete Fourier Transform (DFT), and is implemented in Matlab. The method assumes the velocity profile in a section of a pipe as a superposition of polynomials up to 6th order. Each polynomial component is defined along a specific direction in the plane of the pipe section. For a potential distribution obtained in a uniform magnetic field, this direction is not unique for quadratic and higher-order components; thus, multiple possible solutions exist for the reconstructed velocity profile. A procedure for choosing the optimum velocity profile is proposed. It is applicable for single-phase or two-phase flows, and requires measurement of the potential distribution in a non-uniform magnetic field. The potential distribution in this non-uniform magnetic field is also calculated for the possible solutions using weight values. Then, the velocity profile with the calculated potential distribution which is closest to the measured one provides the optimum solution. The reliability of the method is first demonstrated by reconstructing an artificial velocity profile defined by polynomial functions. Next, velocity profiles in different two-phase flows, based on results from the literature, are used to define the input velocity fields. In all cases, COMSOL Multiphysics is used to model the physical specifications of the EMFM and to simulate the measurements; thus, COMSOL simulations produce the potential distributions on the internal circumference of the flow pipe. These potential distributions serve as inputs for the analytical method. The reconstructed velocity profiles show satisfactory agreement with the input velocity profiles. The method described in this paper is most suitable for stratified flows and is not applicable to axisymmetric flows in its present form. Its novelty is

that it provides not only a mean flow velocity, but a velocity distribution in a circular pipe section as an analytical function of the spatial coordinates.

Keywords: Discrete Fourier Transform, electromagnetic flow measurement, potential distribution, velocity profile

1. Introduction

Electromagnetic flow meters (EMFMs) have been used widely to measure the volumetric flow rate of conducting fluids. The conventional EMFM can have a uniform magnetic field and a pair of point electrodes; one at each end of the diameter normal to the magnetic field direction in a circular pipe. The flow induced voltage U measured between the two electrodes is proportional to the mean flow velocity v_m when the velocity profile is axisymmetric:

$$U = DBv_m \tag{1.1}$$

where D is pipe diameter, and B is magnetic flux density (Shercliff, 1962). In this case, the flow signal of the ideal EMFM depends only on the flow rate, but not on the flow pattern. Bevir (1970) determined the necessary and sufficient condition for this to be satisfied. He also showed that an EMFM with point electrodes could never satisfy this condition, but it could be made insensitive to variations of asymmetric velocity profile if the flow is rectilinear.

Conventional EMFMs have been extended in different ways, in particular, by adding further pairs of electrodes and by creating non-uniform magnetic fields. An approach that is insensitive to the flow velocity profile was proposed by Horner et al. (1996). They extended a conventional system by adding additional pairs of electrodes, and showed a significant improvement in accuracy for eight- or sixteen-electrode EMFMs. Xu et al. (2001) proposed a multi-electrode EMFM. However, they made the assumption that the potential difference, measured between the ends of a chord perpendicular to the magnetic field, is influenced only by the flow velocity components lying on that chord. With reference to Leeungculsatien & Lucas (2013), this assumption is unlikely to be correct. This type of flow meter provides mean velocity and volumetric flow rate in the flow cross section. However, it cannot determine the local axial velocity distribution, which is essential e.g. in multiphase flows in order to find the volumetric flow rate of a particular phase if its local volume fraction distribution is also known.

Teshima et al. (1994) proposed a design of the magnetic field to measure or evaluate flow profile and presented experimental results of flow profile measurement using a rotating magnetic field.

Varying the design of the magnetic field and the electrodes made it possible to apply EMFMs for reconstruction of a flow velocity field in a pipe. Clearly, the dependence of flow induced potentials on flow pattern is essential in order to be able to do this. Xu et al. (2004) developed a modified filtered backprojection algorithm in order to improve the quality of reconstructed velocity profiles in non-axisymmetric flows. Sakuratani & Honda (2010) reconstructed the flow field in partially filled pipes using the weight vector corresponding to water level in the pipe. Leeungculsatien & Lucas (2013) proposed a design of EMFM for reconstructing axial velocity profiles in stratified flows. They divided the pipe section into pixels, and their method provided the axial velocity in each pixel.

The present paper describes an analytical method for reconstruction of velocity profiles from measured potential distributions obtained from a multi-electrode EMFM. The technique is most suitable for stratified flows rather than axisymmetric flows. An alternative technique for axisymmetric flows is published in Zhang & Lucas (2013), whereas the extension of the technique presented here for axisymmetric flows is a subject of future study. The method assumes the velocity profile as a superposition of polynomials up to 6^{th} order. Thus, the velocity profile is obtained as an analytical function of the coordinates, and the velocity can be determined at any position in a pipe section. Section 2 explains the theoretical background of the reconstruction method, and the procedure of reconstruction will be provided in Section 3. The geometry and some specifications of the EMFM considered are described in Section 4. The reconstruction method is initially applied to reconstruct a polynomial velocity profile. Then, the method is tested with more complex velocity profiles measured in two-phase flows in Section 5. Section 6 provides pertinent conclusions.

2. Theoretical Background of Electromagnetic Flow Meters and Reconstruction Method

2.1 Potential Distribution at the Wall of a Circular Pipe

The relationship between a polynomial velocity profile and the potential distribution at the pipe wall will be derived in this section. The pipe is mounted within a Helmholtz coil that provides the magnetic field. The potential distribution is measured by means of electrodes that are placed on the pipe circumference (see Fig. 1b). The pipe is considered to have an infinite length in the axial or *z*-

direction. All the quantities are assumed to be independent of the *z*-direction. The potential distribution at the pipe wall is given by a surface integral over the cross section Ω of the pipe (Shercliff, 1962; Horner et al., 1996):

$$U(\vec{x}') = \iint_{\Omega} \vec{v}(\vec{x}) \cdot \left[\vec{B}(\vec{x}) \times \operatorname{grad} G(\vec{x}, \vec{x}')\right] \mathrm{d}^2 x = \iint_{\Omega} v_z \left(B_x \frac{\partial G}{\partial y} - B_y \frac{\partial G}{\partial x} \right) \mathrm{d}^2 x \tag{2.1}$$

where $\vec{v}(\vec{x}) = [0, 0, v_z]$ is the velocity field which is assumed to have only a component in the *z*-direction, $\vec{B}(\vec{x})$ is the magnetic flux density vector, $G(\vec{x}, \vec{x}')$ is the Green's function of the second kind of the disc Ω with radius R, $\vec{x}'$ is the position of electrodes, and $\vec{x}$ is the integration variable. The assumptions imply that the problem is two dimensional; thus, it is sufficient to consider a section in the (*x*,*y*)-plane. The position and integration variables with polar coordinates are written as follows: $\vec{x}' = R[\cos\theta, \sin\theta]$ and $\vec{x} = r[\cos\vartheta, \sin\vartheta]$. Then, the Green's function takes the form (Morse & Feshbach, 1953):

$$G(r, \vartheta, R, \theta) = -2 \ln R + \frac{1}{\pi} \sum_{k=1}^{\infty} \frac{1}{k} \left(\frac{r}{R} \right)^k \cos k(\vartheta - \theta) \qquad 0 \le \vartheta, \theta < 2\pi \quad \text{and} \quad 0 \le r < R \tag{2.2}$$

The magnetic field is assumed to be homogeneous and applied in the negative *y*-direction, i.e. $\vec{B} = B \cdot [0, -1]$, then the potential becomes:

$$U(\vec{x}) = B \iint_{\Omega} v_z \frac{\partial G}{\partial x} \mathrm{d}^2 x \tag{2.3}$$

or, in polar coordinates after substitution of Eq. (2.2):

$$U(\theta) = \frac{B}{\pi} \int_0^R \int_0^{2\pi} v_z \sum_{k=1}^{\infty} \frac{r^k}{R^k} \cos[(k-1)\vartheta - k\theta] \, \mathrm{d}\vartheta \mathrm{d}r \tag{2.4}$$

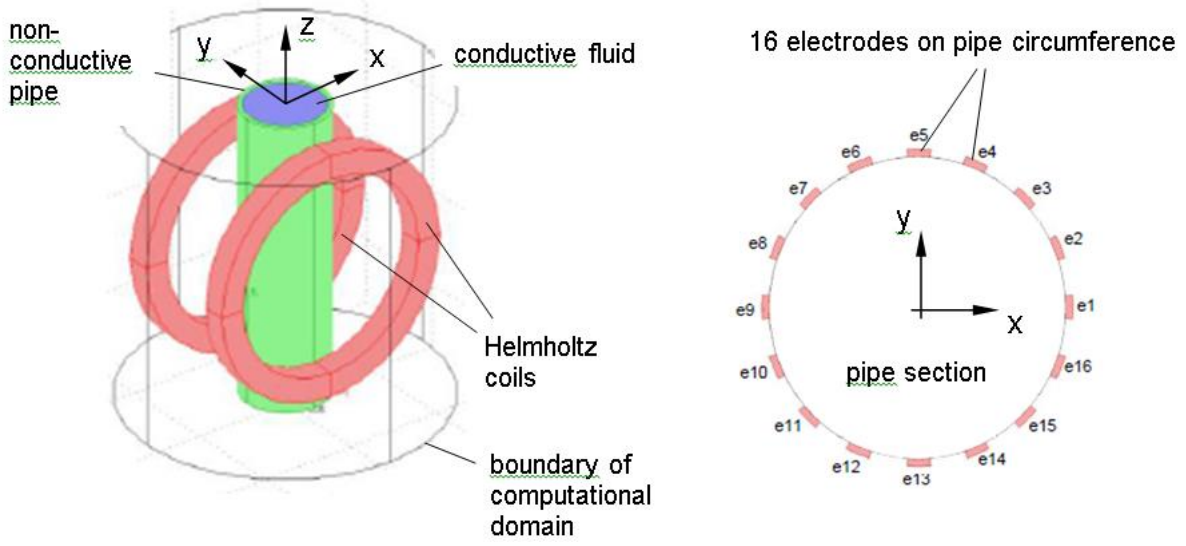

(a) (b)

Fig. 1: Electromagnetic flow meter; (a) geometry and computational domain; (b) position of electrodes

The Fourier series expansion of the velocity field can be written in the form:

$$v_z(r,\vartheta) = \frac{1}{2}c_0(r) + \sum_{k=1}^{\infty} c_k(r)\cos k\vartheta + s_k(r)\sin k\vartheta \tag{2.5}$$

where the coefficients are obtained as follows

$$c_k(r) = \frac{1}{\pi}\int_0^{2\pi} v_z(r,\vartheta)\cos k\vartheta \,\mathrm{d}\vartheta \qquad k = 0,1,2,\ldots \tag{2.6}$$

$$s_k(r) = \frac{1}{\pi}\int_0^{2\pi} v_z(r,\vartheta)\sin k\vartheta \,\mathrm{d}\vartheta \qquad k = 1,2,\ldots \tag{2.7}$$

The potential distribution (2.4) after substitution of the velocity field (2.5) will take the form:

$$U(\theta) = B\left[M_1(c_0)\cos\theta + \sum_{k=1}^{\infty} M_{k+1}(c_k)\cos(k+1)\theta + M_{k+1}(s_k)\sin(k+1)\theta\right] \tag{2.8}$$

with

$$M_{k+1}(c_k) = \int_0^R c_k(r)\left(\frac{r}{R}\right)^{k+1}\mathrm{d}r \qquad k = 0,1,2,\ldots \tag{2.9}$$

$$M_{k+1}(s_k) = \int_0^R s_k(r)\left(\frac{r}{R}\right)^{k+1} \mathrm{d}r \qquad k = 1,2,\ldots \tag{2.10}$$

2.2 Conditions for a Given Polynomial Velocity Profile Component only Giving Rise to a Single Discrete Fourier Transform (DFT) Component

The velocity profile is assumed in a polynomial form. For such functions the coefficients (2.6) and (2.7), together with the potential distribution (2.8), can be determined analytically. The superposition of polynomial components can also be used to approximate more complex velocity profiles. Since the EMFM contains 16 electrodes (N = 16), as will be described in Section 4, polynomials up to 6th order can be reconstructed after applying the Discrete Fourier Transform (see Section 2.3). Suppose the nth-order component of the velocity profile ($0 \le n \le 6$) is in the simple form

$$v_n(x;y) = a_n \frac{\left(x\cos\theta_{Q,n} + y\sin\theta_{Q,n}\right)^n}{R^n} \tag{2.11}$$

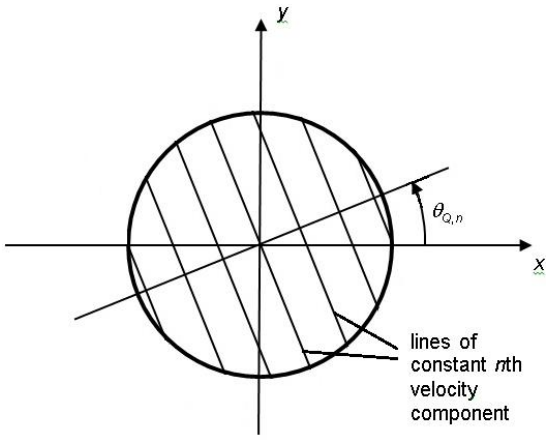

Fig. 2: Definition of the direction $\theta_{Q,n}$

with $\theta_{Q,n}$ denoting the angle of direction with respect to the x-axis, where this component is defined, and a_n is constant. The velocity component, v_n, only changes in the direction $\theta_{Q,n}$ and is constant along lines orthogonal to this direction (see Fig. 2). It should be noted that $\theta_{Q,n}$ is not defined for n = 0, because $v_0 = a_0$ for a uniform velocity profile. The potential distribution for this velocity component becomes

$$U_n(\theta) = \frac{1}{(n+1)2^n} a_{n,n} BR \sum_{k=0}^{\left\lfloor \frac{n}{2} \right\rfloor} \binom{n+1}{k} \left[\cos(n-2k)\theta_{Q,n} \cos(n-2k+1)\theta + \sin(n-2k)\theta_{Q,n} \sin(n-2k+1)\theta \right] \quad (2.12)$$

where

$$\left\lfloor \frac{n}{2} \right\rfloor = \begin{cases} \frac{n}{2} & \text{for } n \text{ is even} \\ \frac{n-1}{2} & \text{for } n \text{ is odd} \end{cases} \quad (2.13)$$

The overall boundary potential distribution $\tilde{U}(\theta)$ is obtained by summing $U_n(\theta)$ for all individual velocity components (e.g. $0 \le n \le 6$). In this case, however, a given component of the DFT of $\tilde{U}(\theta)$ does not relate to a single velocity component, because each velocity component will give rise to multiple frequencies in the boundary potential distribution (see Eq. (2.12)). In order to be able to obtain information about the nth velocity component from the DFT, $U_n(\theta)$ must be expressed only in terms of the trigonometric quantities, $\cos(n+1)\theta$ and $\sin(n+1)\theta$. This will ensure that in the case of several velocity components, each of different order n, the (n+1)th component in the DFT of $\tilde{U}(\theta)$ relates only to the nth order velocity component (see Section 2.3). For the nth order velocity component, in order to eliminate terms other than $\cos(n+1)\theta$ and $\sin(n+1)\theta$, the velocity component has to be written in the form, if n is odd,

$$v_n(x;y) = a_{n,n} \frac{\left(x\cos\theta_{Q,n} + y\sin\theta_{Q,n}\right)^n}{R^n} + a_{n,n-2} \frac{\left(x\cos\theta_{Q,n} + y\sin\theta_{Q,n}\right)^{n-2}}{R^{n-2}} + \ldots + a_{n,1} \frac{x\cos\theta_{Q,n} + y\sin\theta_{Q,n}}{R} \quad (2.14)$$

or, if n is even,

$$v_n(x;y) = a_{n,n} \frac{\left(x\cos\theta_{Q,n} + y\sin\theta_{Q,n}\right)^n}{R^n} + a_{n,n-2} \frac{\left(x\cos\theta_{Q,n} + y\sin\theta_{Q,n}\right)^{n-2}}{R^{n-2}} + \ldots + a_{n,0} \quad (2.15)$$

Thus, the nth velocity component is written as a sum of terms in the form of Eq. (2.14) or (2.15). The coefficients $a_{n,n-2}$, $a_{n,n-4}$, …, $a_{n,1}$ or $a_{n,0}$ may be chosen so that the undesired trigonometric terms will be eliminated. If $m = n/2$ (n is even) and $m = (n-1)/2$ (n is odd), then these conditions are as follows

$$a_{n,n-2} = -\frac{n-1}{4} a_{n,n} \quad (2.16)$$

$$a_{n,n-4} = -\frac{n-3}{(n+1)2^4} \binom{n+1}{2} a_{n,n} - \frac{n-3}{2^2} a_{n,n-2} \quad (2.17)$$

…

$$a_{n,n-2m} = -\frac{(n+1-2m)}{(n+1)2^{2m}}\binom{n+1}{m}a_{n,n} - \frac{(n+1-2m)}{(n-1)2^{2m-2}}\binom{n-1}{m-1}a_{n,n-2} - \frac{(n+1-2m)}{(n-3)2^{2m-4}}\binom{n-3}{m-2}a_{n,n-4} - \ldots$$

$$- \frac{(n+1-2m)}{(n+1-2(m-1))2^{2}}\binom{n+1-2(m-1)}{1}a_{n,n-2(m-1)} \tag{2.18}$$

In this case, the potential distribution associated with the *n*th velocity component will be simplified to the following form which only contains terms in cos(*n*+1)θ and sin(*n*+1)θ

$$U_n(\theta) = K_n\left[\cos n\theta_{Q,n}\cos(n+1)\theta + \sin n\theta_{Q,n}\sin(n+1)\theta\right] \tag{2.19}$$

where

$$K_n = \frac{1}{(n+1)2^n}a_{n,n}BR \tag{2.20}$$

with *B* and *R* standing for the magnetic flux density and pipe radius, respectively. Note that in the presence of multiple velocity components, the overall boundary potential distribution $\tilde{U}(\theta)$ is again given by summing the individual components $U_n(\theta)$ for all relevant values of n.

The coefficient K_n can be obtained from the (*n*+1)th component X_{n+1} of the DFT of the boundary potential distribution $\tilde{U}(\theta)$ using

$$K_n = \pm 2\left|X_{n+1}\right| \tag{2.21}$$

Then, the coefficient $a_{n,n}$ is determined from X_{n+1} as follows

- For uniform (*n* = 0) and linear (*n* = 1) terms, one possibility exists only:

$$a_{0,0} = \mathrm{sgn}(\mathrm{Re}\,X_1)\frac{2}{BR}\left|X_1\right| \tag{2.22}$$

$$a_{1,1} = \frac{8}{BR}\left|X_2\right| \tag{2.23}$$

- For quadratic (*n* = 2) and higher-order (*n* > 2) terms:

$$a_{n,n} = \pm\frac{(n+1)2^{n+1}}{BR}\left|X_{n+1}\right| \tag{2.24}$$

2.3 Application of the DFT to the Boundary Potential Distribution

Once the overall potential distribution $\tilde{U}(\theta)$ is known, information about the velocity profile can be gained by application of the DFT. First, the potential distribution is discretized in order to obtain the

potential U_p (p = 0,…,N-1) at the positions of the measurement electrodes. The DFT of the series U_p then provides a series of N complex numbers as follows

$$X_n = \frac{1}{N}\sum_{p=0}^{N-1} U_p \exp\left(-j\left(2\pi np/N\right)\right) \qquad n = 0,1,\ldots,N-1 \tag{2.25}$$

where N is the number of samples. Note that X_n is associated with the (n-1)th boundary potential component $U_{n-1}(\theta)$ which is in turn associated with (n-1)th velocity component $v_{n-1}(x;y)$. The value of X_n is related to the amplitude and phase of $U_{n-1}(\theta)$. Note also that $U_{n-1}(\theta)$ has a wavelength of $2\pi R/n$. Thus, from the preceding arguments, a uniform velocity component $v_0(x;y)$ gives rise to the boundary potential component $U_0(\theta)$ which undergoes one complete cycle around the boundary. The DFT component associated with this uniform velocity component is X_1. A linear velocity component $v_1(x;y)$ gives rise to a boundary potential component $U_1(\theta)$ which undergoes two complete cycles around the boundary, etc. In case of a multi-electrode EMFM, N is equal to the number of electrodes on the circumference. The argument ψ_n associated with the complex number X_n is determined using

$$\psi_n = \arctan\frac{\mathrm{Im}(X_n)}{\mathrm{Re}(X_n)} \tag{2.26}$$

taking into account the quadrant in which X_n lies. Unique values of X_n exist only up to the Nyquist frequency, that is half of the sampling frequency (i.e. N/2). The numbers X_0 and $X_{N/2}$ are real; thus, the numbers from X_1 to $X_{N/2-1}$ provide information about polynomial components of the velocity profile from 0th (uniform) to (N/2-2)th order.

2.4 Angle of Direction of Velocity Profile

If the velocity profile takes the form (2.14) or (2.15), then the angle $\theta_{Q,n}$ of the direction of velocity component v_n can be determined, as follows, from the argument ψ_n of the complex number X_n.

- If n is odd and $a_n > 0$:

$$\theta_{Q,n} = -\frac{\psi_{n+1}}{n} + \frac{2k\pi}{n} \qquad \theta_{Q,n} \in \left[\frac{(2k-1)\pi}{n}, \frac{(2k+1)\pi}{n}\right) \qquad k = 0,1,\ldots,n-1 \tag{2.27}$$

- If n is odd and $a_n < 0$: the same solutions can be obtained, i.e. there are no further solutions.
- If n is even and $a_n > 0$:

$$\theta_{Q,n} = -\frac{\psi_{n+1}}{n} + \frac{2k\pi}{n} \qquad \theta_{Q,n} \in \left[\frac{(2k-1)\pi}{n}, \frac{(2k+1)\pi}{n}\right) \qquad k = 0,1,\ldots,n/2-1 \tag{2.28}$$

- If n is even and $a_n < 0$:

$$\theta_{Q,n} = -\frac{\psi_{n+1}}{n} + \frac{(2k+1)\pi}{n} \qquad \theta_{Q,n} \in \left[\frac{k2\pi}{n}, \frac{(k+1)2\pi}{n}\right) \qquad k = 0,1,\ldots,n/2-1 \tag{2.29}$$

The equations (2.27) or (2.28)-(2.29) imply that there exist n possible values of $\theta_{Q,n}$ for a velocity component in the form of an nth order polynomial. Consequently, if a velocity profile is composed of the sum of velocity components up to the nth order polynomial, the number of possible solutions for this velocity profile is $n!$ Selection of the optimum solution is described in Section 3.2.

3. Procedure for Reconstruction of Velocity Profiles

3.1 Reconstruction of possible velocity profiles

The procedure to determine the polynomial components of a velocity profile and their directions is summarized by the following stages.

- The nth order polynomial component of the velocity profile is assumed in the form of (2.14) or (2.15) if n is odd or even, respectively.
- The measured overall potential distribution $\tilde{U}(\theta)$ can be written as the sum of a series of components $U_n(\theta)$ given by Eq. (2.19) with (2.20). For a 16-electrode EMFM the maximum allowable value of n is 6 (see Section 2.3), but, if required, n may be limited to a lower value n_{max} if it is deemed unlikely that the velocity profile will contain velocity components of order greater than n_{max}.
- The DFT of the measured potential distribution $\tilde{U}(\theta)$ is obtained giving the DFT components X_n ($n = 1,\ldots,n_{max}+1$).
- The coefficient $a_{n,n}$ is obtained from one of Eqs. (2.22)-(2.24).
- The coefficients $a_{n,n-2}$, …, $a_{n,n-2m}$ are calculated from Eqs. (2.16)-(2.18).
- The possible angles of direction of the nth velocity component are determined from the argument ψ_{n+1} associated with the (n+1)th DFT component X_{n+1} from Eq. (2.27) if n is odd, or from Eqs. (2.28) and (2.29) if n is even.

3.2 Choice of optimum solution

The procedure as described in Section 3.1 provides *n*! velocity profile solutions if all velocity components up to *n*th order are present. Thus, the optimum solution must be chosen from them. A method is proposed in this study for this purpose, which is applicable for single and two-phase flows, and is based on predicting the boundary potential distribution in a non-uniform magnetic field for a given velocity profile using weight values. This non-uniform magnetic field is described later in the present section and shown in Fig. 3b.

This method can be applied to choose the optimum solution if the potential distribution is measured in a specific non-uniform magnetic field, as well as the uniform magnetic field, and the potential distribution is calculated using weight values for all of the possible velocity profile solutions in this non-uniform magnetic field. The optimum velocity profile is that for which the calculated boundary potential distribution most closely matches the measured boundary potential distribution in the non-uniform magnetic field. Before the potential distribution associated with a given velocity profile can be calculated for the non-uniform magnetic field, the relevant weight values must be determined.

In the present study, the pipe section is divided into *M* subdomains (see Fig. 3a, from which it can be seen that *M* = 30). For an *N*-electrode system the potential difference $\hat{U}_j$ between the *j*th electrode and a reference electrode in the non-uniform magnetic field can be expressed as follows

$$\hat{U}_j = \frac{2B_{op}}{\pi R} \sum_{i=1}^{M} v_i w_{ij} A_i \qquad j = 1,\ldots,N-1 \tag{3.1}$$

where A_i is the area of the *i*th subdomain and v_i is the mean axial velocity in the *i*th subdomain calculated using the analytical expression for velocity profile associated with one of the *n*! possible velocity profile solutions. w_{ij} is the weight value relating the velocity in the *i*th subdomain to the *j*th potential difference measurement $\hat{U}_j$, *R* is the internal pipe radius and B_{op} is a reference magnetic flux density at a specific location in the flow cross section for the case of the non-uniform magnetic field.

In this paper simulation results are presented whereby a reference velocity profile is entered into a COMSOL model of a 16-electrode EMFM (see Fig. 1 and Section 4). The potentials U_p (*p* = 0 to 15)

on the 16 electrodes are calculated in a uniform magnetic field of 0.01 T allowing the n! possible predictions of the original reference velocity profile to be calculated as described in Section 3.1. (Note that the uniform magnetic field is obtained by letting equal current of appropriate magnitude flow in the same direction in each of the coils forming the Helmholtz coil).

Next, the same velocity profile is entered into COMSOL but for the case of a non-uniform magnetic field, generated by letting currents of equal magnitude flow in opposite directions in each of the coils forming the Helmholtz coil. The resultant non-uniform magnetic field is shown in Fig. 3b. The value of B_{op} in Eq. (3.1) is arbitrarily taken as the magnetic flux density at electrode e_{13} (Fig. 1b) and in the simulations described in this paper was equal to 0.005 T. For this non-uniform magnetic field the potentials U_p on each of the 16 electrodes were calculated using COMSOL, and 15 reference potential differences $\hat{U}_{j,ref}$ (j = 1 to 15) were obtained by subtracting the value of the potential U_5 (on reference electrode e_5) from the value of the potential on each of the remaining electrodes. Next, for each of the n! velocity profile solutions, the 15 potential differences $\hat{U}_j$ were calculated for the non-uniform magnetic field using the weight value method encapsulated by Eq. (3.1). Finally, for each of the n! velocity profile solutions, a quantity S_U was calculated where

$$S_U = \sum_{j=1}^{15} \left(\hat{U}_{j,ref} - \hat{U}_j \right)^2 \tag{3.2}$$

The optimum velocity profile from the n! possible solutions was taken as that for which the quantity S_U was a minimum, i.e. the velocity profile for which the predicted potential differences using Eq. (3.1) gave the best agreement with the calculated potential differences $\hat{U}_{j,ref}$ which were obtained by applying the reference velocity profile to the COMSOL simulation model.

The weight values w_{ij} in Eq. (3.1) were obtained using a method described in detail by Leeungculsatien & Lucas (2013). This method requires 30 separate COMSOL simulations, one for each of the 30 subdomains shown in Fig. 3a. Each simulation was carried out using the non-uniform magnetic field shown in Fig. 3b and for a given simulation the axial velocity in the chosen subdomain (with index i) was set equal to $v_{wt,i}$ whilst the axial velocity in all of the other subdomains was set equal to zero. The potentials on each of the 16 electrodes calculated using COMSOL were used to generate 15 potential differences $\hat{U}_{wt,j}$ (j = 1 to 15) by subtracting the potential at electrode e_5, successively,

from the potentials on each of the remaining electrodes. The weight values w_{ij} associated with the chosen subdomain with index i were then calculated using the expression

$$w_{ij} = \frac{\pi R}{2B_{op}} \cdot \frac{\hat{U}_{wt,j}}{A_i v_{wt,i}} \qquad i = 1,\ldots,30; \quad j = 1,\ldots,15 \tag{3.3}$$

This process was repeated for the remaining subdomains, thereby allowing the 450 weight values required for the correct application of Eq. (3.1), to be calculated. Due to the high computing time required to calculate the weight values for each subdomain, the number of subdomains was limited to 30 in the present study.

In practical applications of the technique described above measured potentials, obtained from a real EMFM in a uniform magnetic field, are used to generate the $n!$ possible velocity profile solutions. Similarly, measured potentials obtained from the EMFM in a non-uniform magnetic field are used for selecting the optimum velocity profile solution using the weight value method described above. For a given design of EMFM it is only necessary to calculate the weight values once, i.e. prior to the device being used for the first time.

4. Electromagnetic Flow Meter

The geometry of the EMFM considered in the simulations described in this paper is given in this section. It consists of a polytetrafluoroethylene flow pipe mounted within a Helmholtz coil (see Fig. 1a). The inner diameter of the pipe is 80 mm, and the thickness of the pipe wall is 5 mm. The inner and outer diameters of the two coils forming the Helmholtz coil are 204.8 mm and 255 mm, respectively. The potential distribution is measured by means of 16 electrodes that are placed at angular intervals of 22.5 degrees on the pipe circumference as shown in Fig. 1b.

When the weight value method is applied for this specific EMFM, the specifications given in Section 3.2 are considered. Since electrode e_{13} is located at the position $x = 0$, $y = -40$ mm (see Fig. 1), the value of B_{op} in Eq. (3.1) is taken at that position (0.005 T).

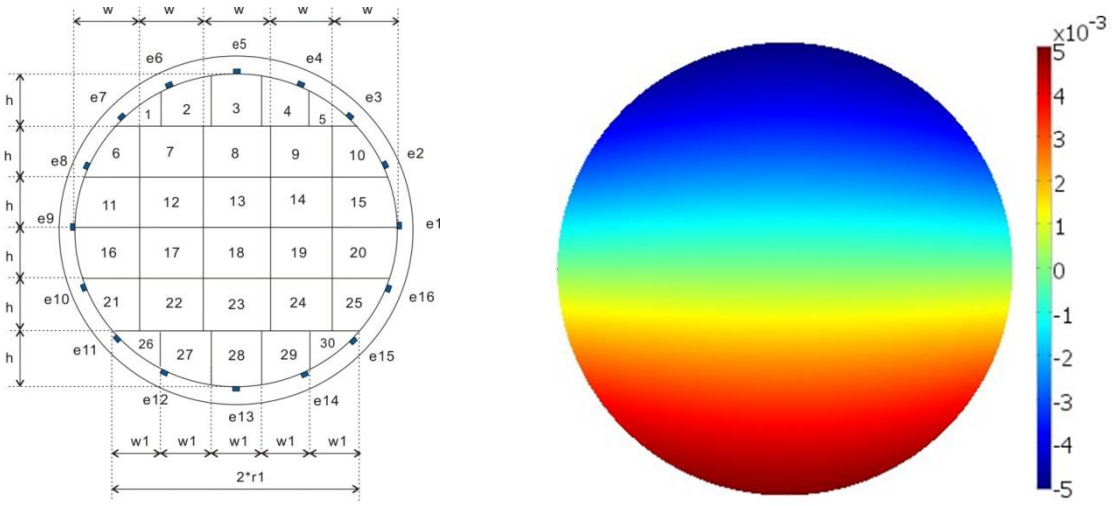

(a) (b)

Fig. 3: Specifications when applying the weight value method, (a) division of pipe section (h = (2*R)/6, w = (2*R)/5, $w1$ = (2*$r1$)/5, where $r1$ = 29.8 mm for a 40-mm-radius pipe), (b) non-uniform magnetic field, colour bar is in T

5. Application of Reconstruction Method

The method applied in this section is to reconstruct different velocity profiles. In this study, COMSOL Multiphysics (COMSOL, 2008) is used to model the physical specifications of the EMFM and to simulate the measurements. The computational domain is shown in Fig. 1a. It should be noted that the pipe was not simulated in its full length in order to reduce computational cost. For each case under consideration, a velocity profile is defined as the input for the COMSOL simulation. The simulation then produces a potential distribution on the internal circumference of the pipe. This potential distribution is used in the reconstruction method described in Section 3 to attempt to reproduce the velocity profile that was initially input into the COMSOL simulation. The reconstruction method was implemented in Matlab.

First, the reconstruction of possible solutions was tested by a known velocity profile defined in polynomial form. Then, the method including the choice of optimum solution was applied to two more complex velocity profiles which had previously been measured in two-phase flows.

5.1 Reconstruction of a quartic velocity profile

The following 4^{th}-order (quartic) polynomial velocity profile was used for testing the reconstruction method

$$v(x;y)=v_0(x;y)+v_1(x;y)+v_2(x;y)+v_3(x;y)+v_4(x;y) \tag{5.1}$$

where the indices refer to the order of polynomial, and the components are defined as follows

$$v_0(x;y)=1$$

$$v_1(x;y)=1\left(\frac{x}{R}\cos 90^\circ+\frac{y}{R}\sin 90^\circ\right)$$

$$v_2(x;y)=1\left(\frac{x}{R}\cos 45^\circ+\frac{y}{R}\sin 45^\circ\right)^2-0.25$$

$$v_3(x;y)=1\left(\frac{x}{R}\cos 20^\circ+\frac{y}{R}\sin 20^\circ\right)^3-0.5\left(\frac{x}{R}\cos 20^\circ+\frac{y}{R}\sin 20^\circ\right)$$

$$v_4(x;y)=1\left(\frac{x}{R}\cos 0^\circ+\frac{y}{R}\sin 0^\circ\right)^4-0.75\left(\frac{x}{R}\cos 0^\circ+\frac{y}{R}\sin 0^\circ\right)^2+0.0625$$

The reference velocity profile defined by Eq. (5.1) is introduced into COMSOL, and the potential distribution in the uniform magnetic field is determined (Fig. 4a). This distribution is used as an input for the reconstruction method to determine the possible solutions for the velocity profile. Since a quartic velocity profile is the subject of reconstruction, the highest order of polynomial component is 4 and the number of possible solutions is 4! = 24. Then, the potential distribution in the non-uniform magnetic field is determined by COMSOL for the original velocity profile. 24 possible solutions for the boundary potential distribution in the non-uniform magnetic field are also calculated using the weight value method given in Section 3.2. The sum of differences S_U as defined by Eq. (3.2), is calculated for each of the 24 possible velocity profile solutions, and the optimum velocity profile is the one for which S_U has a minimum value. Fig. 4b shows potential distributions obtained in the non-uniform magnetic field: the distribution simulated by COMSOL is indicated by “COMSOL”, the optimum velocity profile solution chosen as explained above is indicated by “Closest calculated”, and the solution for which S_U is maximum is indicated by “Farthest calculated”. It can clearly be seen that, although both calculated potential distributions are close to that obtained from COMSOL, the “Closest calculated” shows a closer agreement with the COMSOL one than the “Farthest calculated”; the quantity S_U is $2.95\cdot10^{-8}$ and $8.87\cdot10^{-8}$ for the “Closest calculated” and “Farthest calculated” velocity profiles respectively. The corresponding three velocity profiles are drawn in Fig. 5. The chosen solution coincides closely with the reference solution, although some minor differences are visible. However, the farthest calculated solution shows more significant discrepancies from the reference velocity profile.

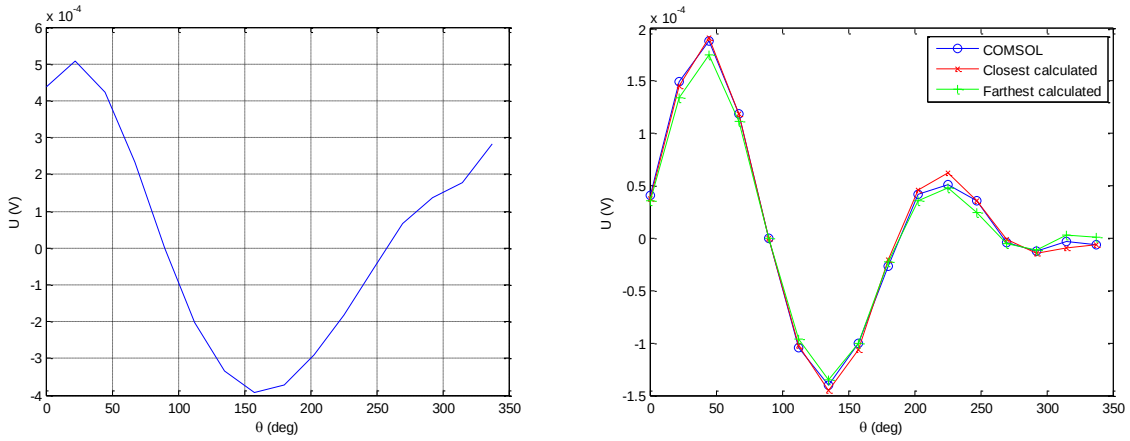

(a) (b)

Fig. 4: Potential distribution of simulated and reconstructed quartic polynomial velocity profiles; (a) uniform magnetic field; (b) non-uniform magnetic field

The reliability of the method may be evaluated by calculating a term δv which represents an average percentage deviation in the local velocity of a reconstructed velocity profile as compared with the original velocity profile. This term δv is determined for each velocity profile solution according to Eq. (5.2):

$$\delta v = \frac{\Delta v_{average}}{v_{in,\max} - v_{in,\min}} = \frac{\sum_{i=1}^{\tilde{M}} \left| v_i - v_{in,i} \right|}{\tilde{M}\left(v_{in,\max} - v_{in,\min} \right)} \cdot 100\% \qquad (5.2)$$

Here, $\tilde{M}$ is a number of subregions into which the cross section can be divided and where the velocity is calculated. In this case, $\tilde{M}$ can be chosen arbitrarily high, because both the input and reconstructed velocity profiles are known analytically. In the example given here $\tilde{M}$ was chosen to be 88. $v_{in,i}$ is the input velocity in the ith subregion. $v_{in,max}$ and $v_{in,min}$ are, respectively, the maximum and minimum velocities in the input velocity profile. [Note that $v_{in,\max} - v_{in,\min}$ is used in the denominator of Eq. (5.2) rather than $v_{in,i}$ to prevent δv tending to ∞ for $v_{in,i}$ values which approach zero]. For the chosen optimum solution (Fig. 5b), the following value was obtained: δv = 2.4%, whereas for the farthest calculated solution (Fig. 5c): δv = 9.2%. Thus, δv is significantly lower for the chosen solution than for the farthest calculated solution; furthermore, the value of δv is smallest for the optimum solution among all the 24 possibilities.

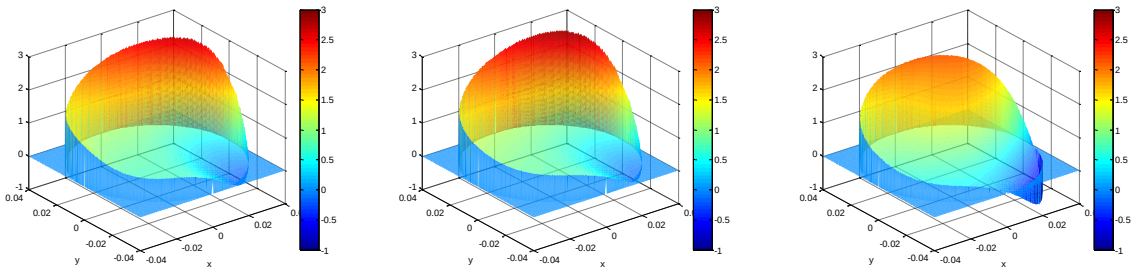

(a) (b) (c)

Fig. 5: Simulated and reconstructed quartic polynomial velocity profiles, *x* and *y* are in m, colour bar is in m/s; (a) reference velocity profile; (b) chosen optimum (closest calculated); (c) farthest calculated

The robustness of the method was studied by adding "noise" to the potential distributions obtained in both the uniform and non-uniform magnetic fields. A random error of up to $\pm 0.01\varepsilon_u$ was added to the calculated true potential at each electrode, using COMSOL for the uniform magnetic field, where $\varepsilon_u = 9 \cdot 10^{-4}$ V. The value of ε_u was chosen because it represents the difference between the true maximum and true minimum electrode potentials in the uniform magnetic field. [Note that this random, absolute error represents a percentage error of up to about $\pm 2\%$ of the true electrode potential for those electrodes with the highest magnitude flow induced potentials. However, for those electrodes with lower magnitude flow induced potentials, the percentage error of the true electrode potential, caused by the addition of $\pm 0.01\varepsilon_u$, may exceed $\pm 10\%$]. Similarly a random error of up to $\pm 0.01\varepsilon_{nu}$ was added to the true potential at each electrode, calculated using COMSOL for the non-uniform magnetic field, where $\varepsilon_{nu} = 3.3 \cdot 10^{-4}$ V. The value of ε_{nu} was chosen because it represents the difference between the true maximum and true minimum electrode potentials in the non-uniform magnetic field. Next, the reconstruction method was applied using these "noisy" potential distributions, and the value of δv was calculated using Eq. (5.2). This process was repeated over 20 trials, since the "noisy" potential distributions, and consequently δv, are slightly different in each trial. The average value of δv in these trials was 4.0%, with a minimum of 2.6%, and a maximum of 5.9%. Note that the δv value was 2.4% for the noise-free potential distributions. These results demonstrate that, for a future practical system, provided that the electrode potentials can be measured to an accuracy of $\pm 0.01\varepsilon_u$ and $\pm 0.01\varepsilon_{nu}$ in the uniform and non-uniform magnetic fields respectively, the mean

deviation δv (Eq. (5.2)) in the local velocity will be of the order of only 4%. In what follows, the reliability of the method will be tested on velocity profiles that are not exactly polynomial.

5.2 Reconstruction of velocity profile measured in two-phase flows

The reconstruction method is applied in this section for two measured velocity profiles, namely the water velocity profile in a two-phase flow of oil in water and the water velocity profile in a two-phase flow of solids in water.

5.2.1 Two-phase flow of oil in water

Two-phase flow of oil in water in a pipe with inclination angle of 30 deg to the vertical was considered in Zhao & Lucas (2011). They measured the volumetric flow rate of water Q_w and of oil Q_o, the time averaged distribution of the local oil volume fraction α_o and the time averaged distribution of the local axial oil velocity v_o, as shown in Fig. 6. The local water velocity v_w is calculated from the local oil velocity v_o using

$$v_w = v_o - v_{slip} \tag{5.3}$$

where the axial slip velocity v_{slip} in a pipe with inclination angle of 30 deg to the vertical is assumed to be given by

$$v_{slip} = v_{slip,0} \cos 30^\circ \tag{5.4}$$

The value for $v_{slip,0}$ was obtained experimentally as 0.16 m/s (Zhao & Lucas, 2011), hence v_{slip} = 0.14 m/s. The input water velocity data in reduced spatial resolution as entered into COMSOL is shown in Fig. 7a. The differences between Figs. 6b and 7a are that the constant slip velocity given by Eq. (5.4) is subtracted and that the spatial resolution is reduced in Fig. 7a. The input velocity profile for the COMSOL simulation shown in Fig. 7a is defined as follows. An 80-mm x 80-mm rectangular section including the circular pipe is divided into 100 identical regions. Three regions at each corner of the rectangular section fall outside the pipe where the velocity is zero (entirely white rectangles in Fig. 7a), and average water velocities were defined in the remaining 88 regions. Of each region, only the area that falls inside the pipe is considered in the calculation (non-white areas of rectangles in Fig. 7a). Average velocities in each region are determined in correspondence with measured values. These values are represented by the colourmap in Fig. 7a. In this section, the potential distribution

that is used in the reconstruction is obtained from a COMSOL simulation in a uniform magnetic field (see also Fig. 7b) using the input velocity profile described above as shown in Fig. 7a.

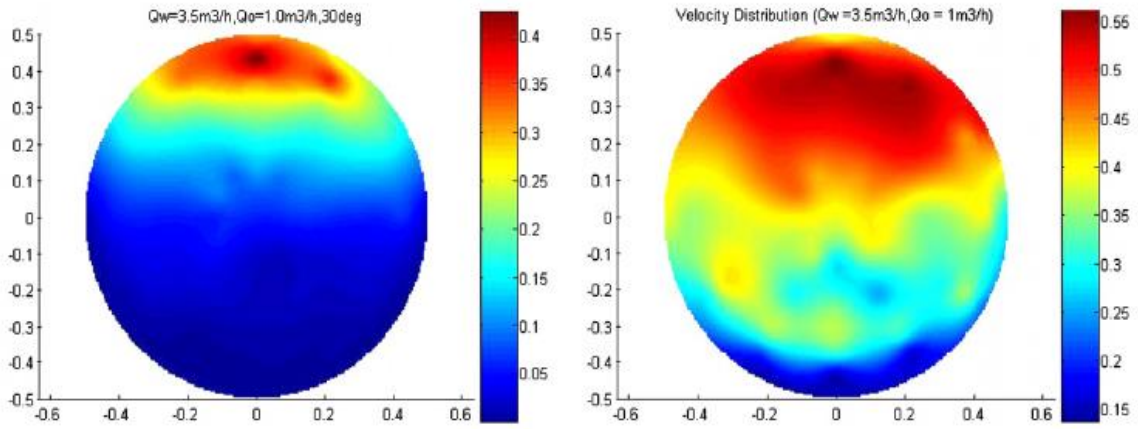

(a) (b)

Fig. 6: Measurements in a two-phase flow of oil-in-water in a pipe with inclination angle of 30 deg to the vertical (from Zhao & Lucas, 2011), horizontal and vertical axes are in m, (a) time averaged distribution of the local oil volume fraction, colour bar represents fraction, (b) time averaged distribution of the local axial oil velocity, colour bar is in m/s

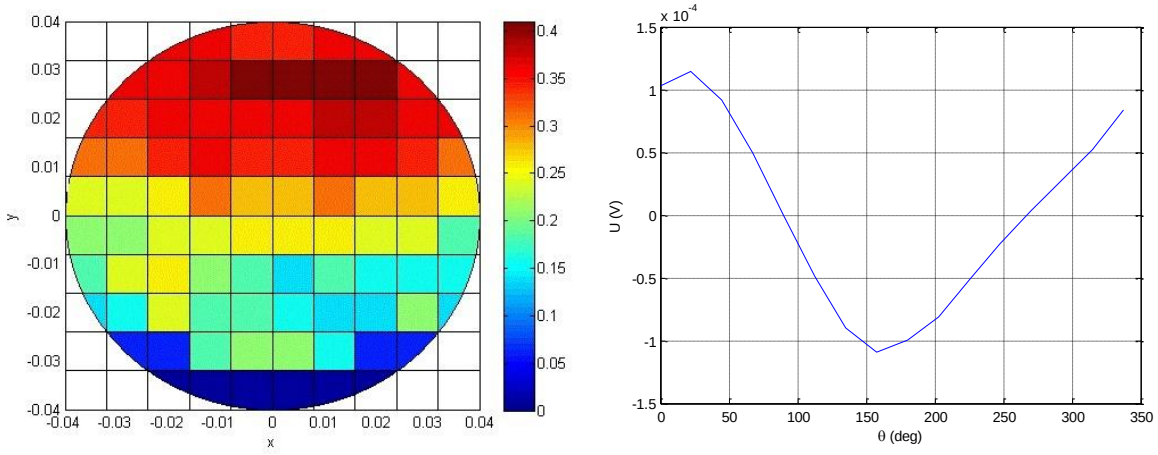

(a) (b)

Fig. 7. (a) Division of pipe section and the discrete input water velocity profile, *x* and *y* are in m, colour bar is in m/s, (b) potential distribution as obtained in COMSOL simulation in a uniform magnetic field

A preliminary study was undertaken to investigate the highest order polynomial velocity component that should be used in the velocity profile reconstruction. To this end, the highest order component was successively changed from first order, to second, to fourth to sixth order. For the velocity profile containing velocity components up to first order only one solution exists, whereas in the other three cases, multiple velocity profile solutions exist. For each case, the solution for which δv, as defined by Eq. (5.2), was a minimum was chosen. These resultant velocity profiles are shown in Fig. 8. The values of δv for these four profiles are 11.01%, 9.02%, 6.75% and 7.91% (for highest order velocity components of first order, second order, fourth order and sixth order, respectively). Inspection of Fig. 8 shows that the velocity profile containing components up to sixth order displays ~~physically unrealistic~~ spatial variations which ~~were~~ are also discrepant with the input velocity profile (Fig. 7a). Note that an earlier series of simulations with a variety of input velocity profiles also showed that, for velocity components of higher order than fourth, δv values started to increase showing that the velocity profile was becoming less accurate. A probable explanation of this observation lies in the tendency of the relative magnitude of DFT components to decrease with increasing 'component number' - the magnitude of the 7th DFT component (corresponding to the 6th order velocity component) being 2 to 3 orders of magnitude smaller than the first components (corresponding to the lowest order velocity components). Thus, noise from any source (numerical or experimental), has a significant effect on the calculated highest order velocity components. Until these noise sources are better understood, the authors have decided to limit the highest order velocity component to fourth order. Consequently, in the analyses which follow, velocity component terms up to fourth order only will be considered.

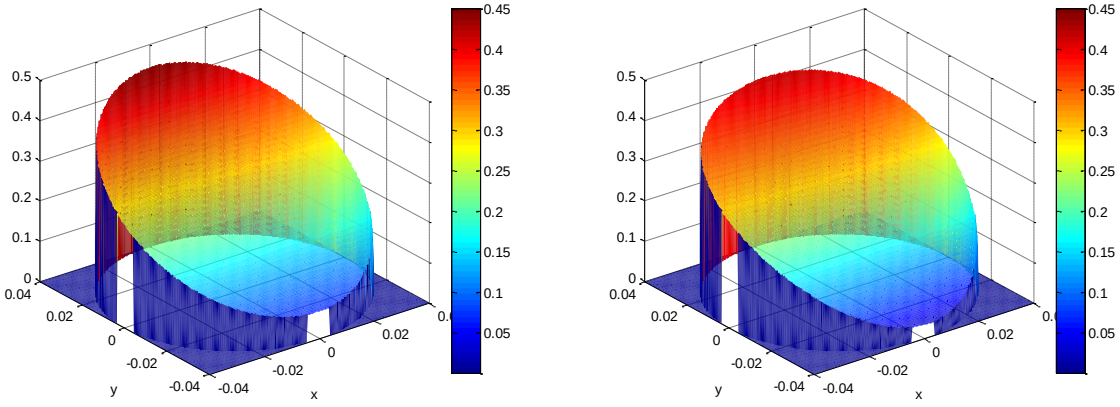

(a) (b)

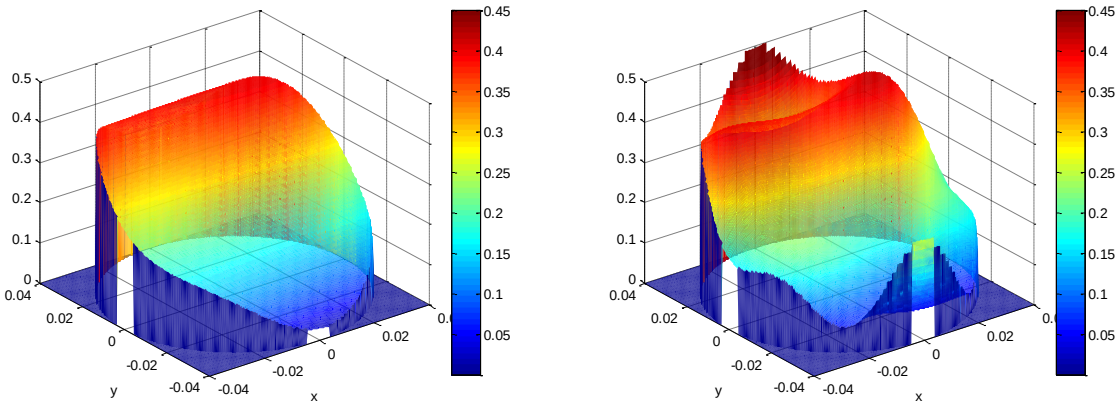

(c) (d)

Fig. 8: Reconstructed water velocity profiles with highest-order terms (a) 1st order, (b) 2nd order, (c) 4th order, (d) 6th order, *x* and *y* are in m, colour bar is in m/s

Using the boundary potential distribution of Fig. 7b, the reconstruction method described in Section 3 was applied to determine the 24 possible water velocity profile solutions. The weight value method described in Section 3.2 (and also in Section 5.1) was then used in order to select the optimum water velocity profile. The optimum oil velocity profile can be obtained by adding the slip velocity v_{slip} to the optimum water velocity profile. It can be seen in Fig. 9 that the potential distribution for the chosen water velocity profile solution ("Closest calculated") provides a closer agreement with the reference water velocity profile than the "Farthest calculated". Note also that the quantity S_U is $2.80 \cdot 10^{-9}$ and $5.01 \cdot 10^{-9}$ for the "Closest calculated" and "Farthest calculated" profiles respectively. However, the difference between the "closest" and "farthest" solutions is less than the difference between the chosen ("Closest calculated") and the reference solutions. The original and the chosen oil velocity profiles are shown in Figs. 10a and 10b, respectively. The term δv as defined by Eq. (5.2) is lowest for the oil velocity profile solution shown in Fig. 10c, whereas it is greatest for the solution shown in Fig. 10d. Consequently, a solution (Fig. 10c) closer to the original oil velocity profile than the chosen solution (Fig. 10b) exists. The value of δv for the oil velocity profile in Fig. 10c is 6.8%. The value of δv for the oil velocity profile in Fig. 10d is 11.4%. The value of δv for the chosen oil velocity profile is 9.0%. Thus, δv is quite low for all the 24 possible solutions. Although it is not minimum for the chosen solution (Fig. 10b), it is below 10% which is still acceptable, and the chosen solution approximates

closely the main characteristics in the original oil velocity profile, without being able to predict some of the more subtle details that are visible in Fig. 10a.

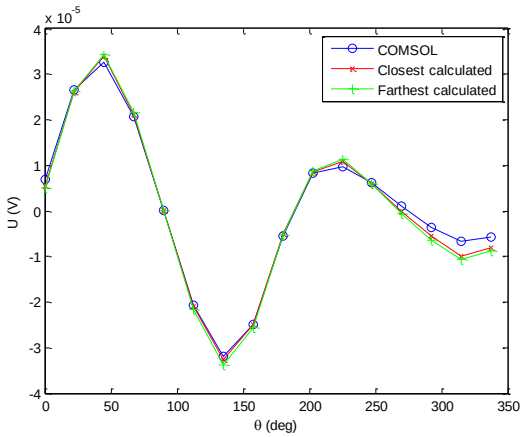

Fig. 9: Potential distribution of simulated and reconstructed velocity profiles in non-uniform magnetic field

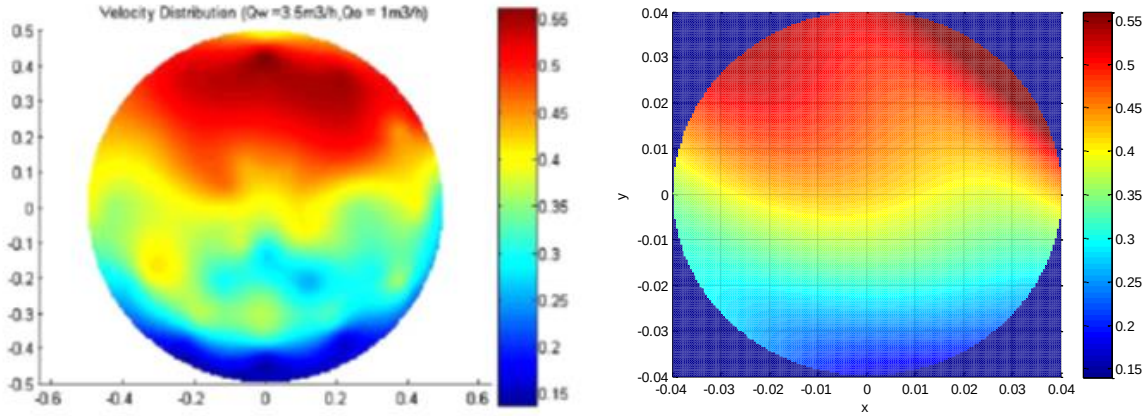

(a) (b)

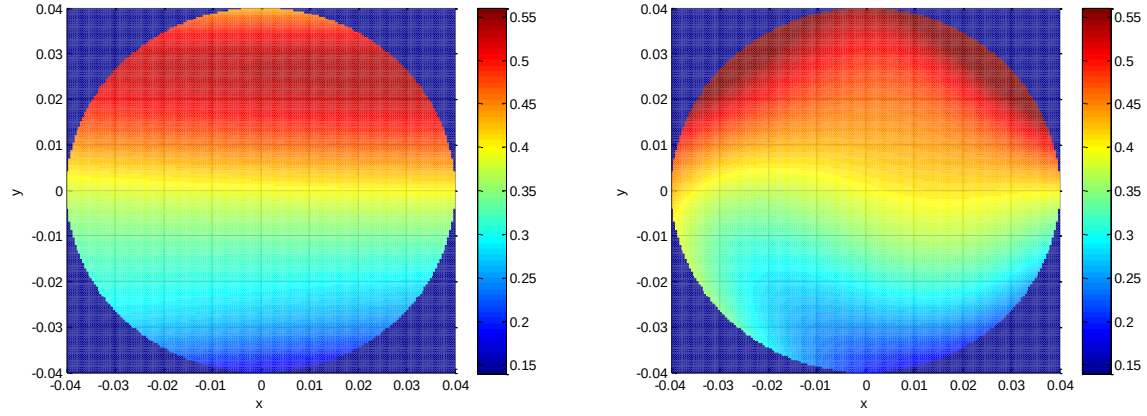

(c) (d)

Fig. 10: Oil velocity profiles, x and y are in m, colour bar is in m/s, (a) original from measurement; (b) chosen by comparing potential distributions (min S_U); (c) lowest value of δv (Eq. 5.2), (d) highest value of δv

5.2.2 Two-phase flow of solids in water

The solids velocity profile for a two-phase flow of solids in water in an inclined pipe with inclination angle of 30 deg to the vertical was measured in Cory (1999). The measured solids velocity profile is shown in Fig. 11. The water velocity profile can be determined from the measured solids velocity profile using Eq. (5.3) with oil velocity v_o replaced by solids velocity. The slip velocity of the solids with respect to water in a vertical pipe was found by Cory (1999) to be $v_{slip,0} = -0.16$ m/s. This value is negative since the solids density was greater than that of water. The application of Eq. (5.4) provides the solids slip velocity in the inclined pipe as $v_{slip} = -0.14$ m/s. The division of pipe section into a number of regions in order to provide the input water velocity profile for a COMSOL simulation was performed in the same way as explained in Section 5.2.1. Potential distributions were obtained from this COMSOL simulation for both the uniform and non-uniform magnetic fields described in Section 3.2.

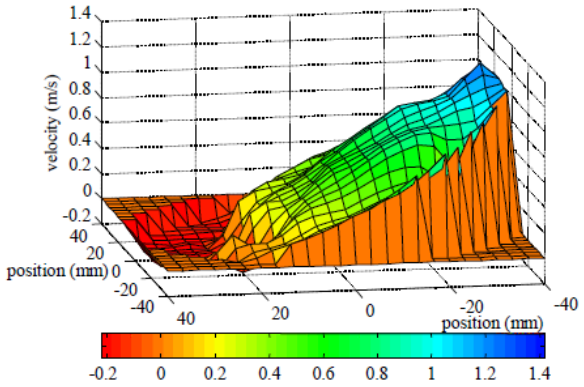

Fig. 11: Measured solids velocity profile (from Cory, 1999)

For the reconstruction procedure water velocity profiles containing polynomial components up to fourth order were considered. The optimum water velocity profile from the 24 possible solutions was chosen by comparing the potential distributions calculated using the weight value method for the non-uniform magnetic field with the reference potential distribution obtained from COMSOL in the non-uniform magnetic field. The potential distribution for the chosen solution in Fig. 12 ("Closest

calculated") provides a closer agreement with the COMSOL simulation than the "Farthest calculated". Note also that the quantity S_U is $2.85 \cdot 10^{-8}$ and $5.55 \cdot 10^{-8}$ for the "Closest calculated" and "Farthest calculated" solutions respectively. The difference between the "closest" and "farthest" potential distributions is less at some angular positions (270-350 deg) than the difference between the "chosen" and the reference potential distributions. However, in this example there are some angular positions where this situation is reversed (20-50 deg, 120-240 deg). The original, "closest calculated" and "farthest calculated" water velocity profiles are shown in Figs. 13a, 13c and 13d, respectively. Also shown, in Fig. 13b, is the water velocity profile for which δv (Eq. 5.2) is a minimum. Similar conclusions can be drawn from Fig. 13 as from Fig. 10 in the previous example. The chosen ("closest calculated") solution (Fig. 13c) provides a visibly closer approximation to the reference water velocity profile (Fig. 13a) than the "farthest calculated" (Fig. 13d). However, the value of δv is lowest for the solution in Fig. 13b, i.e. a solution closer to the original water velocity profile than the "chosen" water velocity profile exists. The value of δv for the profile in Fig. 13b is 5.0%, whereas δv = 5.2% for the chosen solution in Fig. 13c.

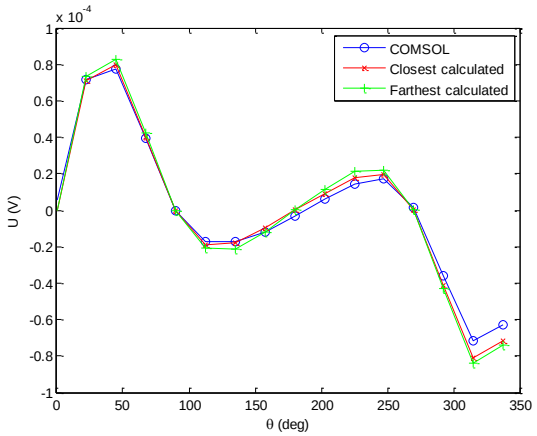

Fig. 12: Potential distribution of simulated and reconstructed water velocity profiles in non-uniform magnetic field

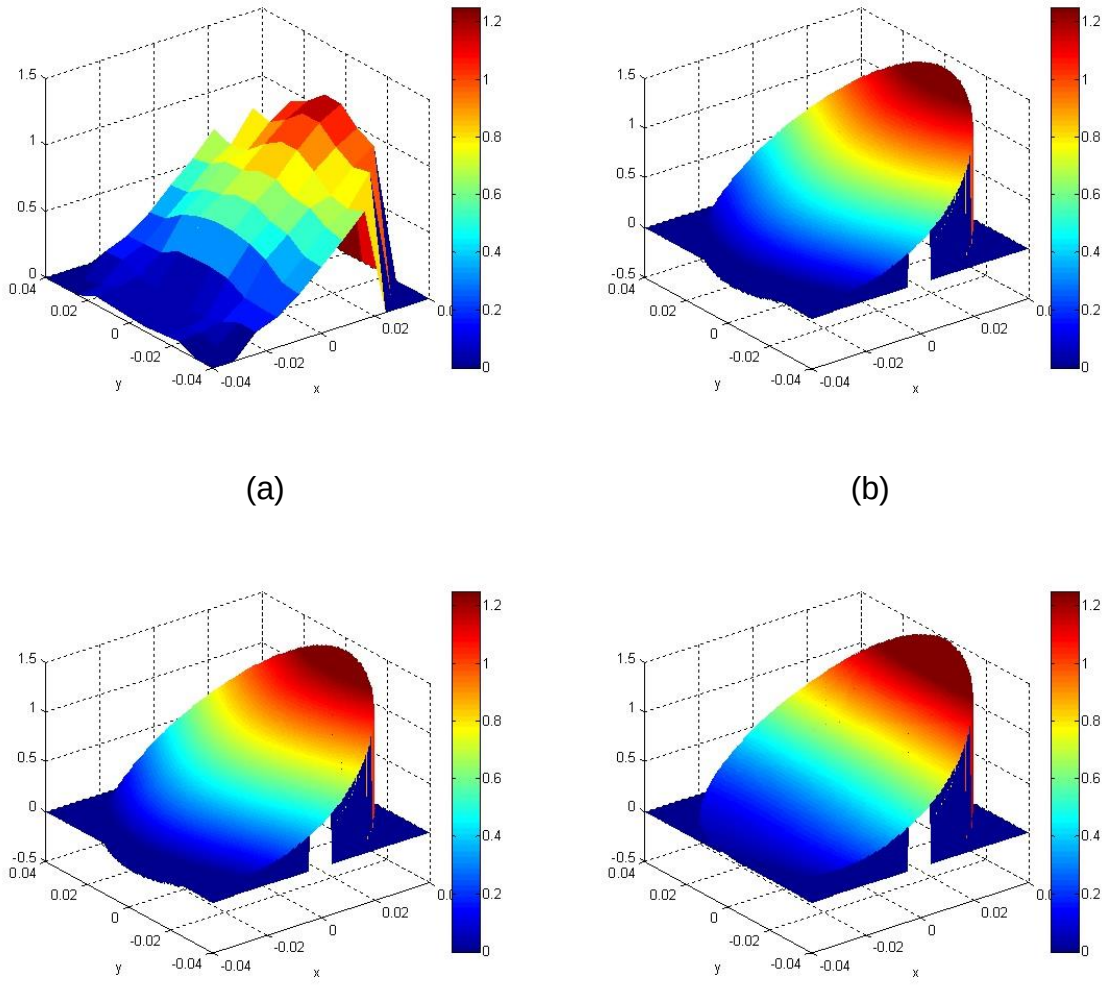

Fig. 13: Water velocity profiles; (a) original as defined in COMSOL simulation; (b) lowest value of δv (Eq. 5.2), (c) "closest calculated" solution by comparing potential distributions (min S_U), (d) "farthest calculated" solution by comparing potential distributions (max S_U)

The results for the two examples presented in this section show that the method proposed for choosing the optimum solution does not necessarily provide the solution with the closest velocity profile to the original velocity profile. However, the chosen solution in both examples provides an estimation of the reference velocity profile for which the mean deviation δv (Eq. 5.2) is below 10%. For many industrial multiphase flow measurement applications this level of error would be acceptable.

6. Conclusions

An analytical velocity reconstruction method has been developed and tested, which is applicable to flow measurement with a multi-electrode electromagnetic flow meter (EMFM). The method is based on the Discrete Fourier Transform (DFT), and includes two steps. Firstly, possible solutions are determined in polynomial form and secondly the optimum velocity profile is chosen from among them. The first step requires measurement of potential distribution in a uniform magnetic field; whereas measurement of potential distribution in a non-uniform magnetic field is necessary for the second step. It was shown that the complex numbers obtained from the DFT coefficients provide information about the coefficients of the polynomial velocity components of the reconstructed velocity profile, together with the angle of the direction of these velocity components. Thus, a method has been proposed that provides the velocity distribution analytically for a continuous conductive phase in a circular pipe section, in either single phase or multiphase flow.

The application of the method to artificial velocity profiles constructed from polynomial velocity components shows that the reconstructed velocity profile coincides closely with the original profile, in spite of the fact that there exist multiple solutions with identical potential distributions in a uniform magnetic field and with nearly identical potential distributions in the non-uniform magnetic field. When the method is applied to more complex velocity profiles, then the choice among the possible solutions may not be that which is closest by local velocities, i.e. that for which the term δv is minimum. However, the chosen solution is a satisfactory estimation of the input velocity profile with a value of δv that in general is not greater than 10%.

References

Bevir, M.K. (1970) The theory of induced voltage electromagnetic flowmeters, *J. Fluid Mech.*, 43(3), 577-590.

COMSOL Multiphysics User's Guide, Version 3.5. COMSOL AB, 2008.

Cory, J. (1999) The Measurement of Volume Fraction and Velocity Profiles in Vertical and Inclined Multiphase Flows, Ph.D. thesis, University of Huddersfield, Huddersfield, UK.

Horner, B., Mesch, F., Trachtler, A. (1996) A multi-sensor induction flowmeter reducing errors due to non-axisymmetric flow profiles. *Meas. Sci. Technol.*, 7, 354-360.

Leeungculsatien, T., Lucas, G.P. (2013) Measurement of Velocity Profiles in Multiphase Flow using a Multi-Electrode Electromagnetic Flow Meter. *Flow Measurement and Instrumentation*, 31, 86-95.

Morse, P.M., Feshbach, H. (1953) *Methods of Theoretical Physics, Part II*, McGraw-Hill, New York, NY.

Sakuratani, M., Honda, S. (2010) Partially Filled Flow Tomography with Electro-Magnetic Induction, *SICE Annual Conference 2010*, Taipei, Taiwan, 2758-2762.

Shercliff, J.A. (1962) *The Theory of Electromagnetic Flow-Measurement*, Cambridge University Press, Cambridge, UK.

Teshima, T., Honda, S., Tomita, Y. (1994) Electromagnetic Flowmeter with Multiple Poles and Electrodes, *Proc. IMTC '94*, Hamamatsu, Japan, THPM 1-5.

Xu, L.J., Li, X.M., Dong, F., Wang, Y., Xu, L.A. (2001) Optimum estimation of the mean flow velocity for the multi-electrode inductance flowmeter, *Measurement Science and Technology*, 12, 1139-1146.

Xu, L., Wang, Y., Dong, F. (2004) On-Line Monitoring of Nonaxisymmetric Flow Profile with a Multielectrode Inductance Flowmeter, *IEEE Transactions on Instrumentation and Measurement*, 53(4), 1321-1326.

Zhang, Z., Lucas, G.P. (2013) Determination of power law velocity profiles by electromagnetic flow measurement. *Proc. 7th World Congress on Industrial Process Tomography (WCIPT7)*, Krakow, Poland, 747-756.

Zhao, X., Lucas, G.P. (2011) Use of a novel dual-sensor probe array and electrical resistance tomography for characterisation of the mean and time-dependent properties of inclined, bubbly oil-in-water pipe flows. *Meas. Sci. Technol.*, 22.